Tcf3 promotes cell migration and wound repair through regulation of lipocalin 2

Qi Miao,Amy T. Ku,Yudai Nishino,Jeffrey M. Howard,Ajay S. Rao,Timothy M. Shaver,Gloria E. Garcia,Diep N. Le,Kristen L. Karlin,Thomas F. Westbrook,Valeria Poli,Hoang Nguyen

Tcf3 promotes cell migration and wound repair through regulation of lipocalin 2

NATURE COMMUNICATIONS (2014) 5
DOI: 10.1038/ncomms5088

Tcf3 promotes cell migration and wound repair through regulation of lipocalin 2

Qi Miao[1], Amy T. Ku[1-2], Yudai Nishino[1], Jeffrey M. Howard[1-3], Ajay S. Rao[1], Timothy M. Shaver[1], Gloria E. Garcia[1], Diep N. Le[1], Kristen L. Karlin[4-5], Thomas F. Westbrook[4-7], Valeria Poli[11] and Hoang Nguyen[1-2,7-10,*]

Baylor College of Medicine, Houston, TX 77030
One Baylor Plaza, BCM 505
Houston, TX 77030
[1]Stem Cells and Regenerative Medicine Center
[2]Interdepartmental Program in Translational Biology and Molecular Medicine
[3]Medical Scientist Training Program
[4]Verna & Marrs McLean Department of Biochemistry & Molecular Biology
[5]Department of Molecular & Human Genetics
[6]Department of Pediatrics
[7]Dan L. Duncan Cancer Center
[8]Department of Molecular and Cellular Biology
[9]Department of Dermatology
[10]Program in Developmental Biology

[11]Molecular Biology Center
University of Turin, Turin, Italy

[*]Correspondence should be addressed to: H.N. (email: hoangn@bcm.edu)

(Keywords: Tcf3, Stat3, lipocalin 2, cell migration, wound healing, keratinocytes)

Cell migration is an integral part of re-epithelialization during skin wound healing, a complex process involving molecular controls that are still largely unknown. Here we identify a novel role for Tcf3, an essential transcription factor regulating embryonic and adult skin stem cell functions, as a key effector of epidermal wound repair. We show that Tcf3 is upregulated in skin wounds and that Tcf3 overexpression accelerates keratinocyte migration and skin wound healing. We also identify Stat3 as an upstream regulator of Tcf3. Mechanistically, we show that the pro-migration effects of Tcf3 are non-cell autonomous and occur independently of its ability to interact with the canonical Wnt effector β-catenin. Finally, we identify Lipocalin-2 downstream of Tcf3 as the key secreted factor that promotes cell migration *in vitro* and wound healing *in vivo*. Our findings provide new insights into the molecular controls of wound-associated cell migration and identify potential therapeutic targets for the treatment of defective wound repair.

Cutaneous wound repair is an essential regenerative process, which is required to maintain the barrier function of the skin after damage. This regenerative process is complex with multiple steps that require dynamic interaction of many cell types[1]. Wound healing proceeds in three partially overlapping phases: (1) inflammation, (2) re-epithelialization, and (3) tissue remodeling. In the re-epithelialization step, epidermal cells migrate into the wound site, proliferate and differentiate to reform the epidermal barrier. Defects in cell migration often lead to defective wound repair[2-7]. Despite the importance of the re-epithelialization step in the wound healing process, our understanding of the molecular control of this crucial step is still lacking.

Tcf3 (also known as Tcf7l1) belongs to the Lef/Tcf family of transcription factors, all of which contain a highly conserved HMG domain that binds to a conserved recognition sequence, as well as domains that interact with the transcriptional activator β-catenin and Groucho/TLE-family corepressors. Lef/Tcf members can function as repressors when bound to Groucho/TLE corepressors or as activators when bound to β-catenin[8,9]. In the absence of Wnt ligand, cytoplasmic β-catenin is phosphorylated by the Apc/Axin complex and targeted for degradation. Binding of Wnt ligands to their surface receptors results in the sequestration of components of the Apc/Axin complex, preventing degradation of β-catenin and allowing its translocation into the nucleus. In most cases, nuclear β-catenin interacts with Lef/Tcf members to activate transcription, converting them from corepressors into coactivators.

Tcf3 seems to be distinct from the other Lef/Tcf members. Although Tcf3 can bind to β-catenin, its major function throughout development appears to be Groucho/TLE-dependent corepression of transcription[10-14]. Tcf3 is expressed in many types of stem cells including embryonic stem cells[11,15] and adult hematopoietic[16,17], neural[16,18] and skin

stem cells[19,20]. Loss of function of Tcf3 leads to gastrulation defects and embryonic lethality[21]. In skin, Tcf3 is expressed in embryonic epidermal cells and adult quiescent stem cells located in the hair follicle bulge region, as well as proliferative migrating stem cell progeny[19,20]. Overexpression of Tcf3 in the epidermis blocks terminal differentiation and maintains cells in an undifferentiated state[20,22]. The expression pattern of Tcf3 in skin is mirrored by its closely related paralog Tcf4 (also known as Tcf7l2), which appears to possess similar functions and can compensate for the absence of Tcf3 in skin development. Loss of both Tcf3 and Tcf4 in skin results in hair follicle morphogenesis defects, as well as failure of re-epithelialization during wound repair and a loss of long-term proliferation/self-renewal[23].

Because the re-epithelialization process during wound repair depends on cell proliferation as well as migration, it is not clear whether Tcf3 has a role in controlling cell migration in addition to its established role in cell proliferation. In this study, we aimed to investigate the role of Tcf3 in wound repair. We found that Tcf3 promotes epidermal cell migration and accelerates wound healing. We also showed that Tcf3's induction in response to wound stimuli is dependent on Stat3, a transcription factor that has previously been shown to be required for efficient wound repair. Finally, we identified lipocalin 2 (Lcn2) as the critical downstream target of Tcf3 that promotes cell migration and wound healing.

RESULTS

Tcf3 is induced at the wound edge and its overexpression promotes cell migration *in vitro*

Since the re-epithelialization process is defective in skin lacking Tcf3 and Tcf4, to explore Tcf3's role in wound healing, we first examined the expression pattern of Tcf3

following full thickness skin wounding in young adult mice. Within 3 days after wounding, Tcf3 is detectable at the wound edge in K5+ cells, with maximal expression levels by day 5 (Fig. 1A). As expected, Tcf3 is not detectable at the wound edge in Tcf3 conditional knockout skin. Unlike Tcf3, other Lef/Tcf members are not induced at the wound edge, including Tcf4, which is otherwise expressed in a similar pattern to Tcf3[23]. Lef1 and Tcf1 (also known as Tcf7), which have dissimilar expression patterns and functions to Tcf3 in adult skin, are also unaffected by wounding (Supplemental Fig. S1).

In the re-epithelialization step of the wound repair process, epidermal cells migrate into the wound site, proliferate and differentiate to reform the epidermal barrier[1]. To determine whether Tcf3 is involved in cell migration, we applied an established *in vitro* cell migration/wounding assay[24] to uncouple cell migration from growth and differentiation effects. In this assay, scratch "wounds" are created in monolayers of mitotically-inactivated mouse keratinocytes, and migration of keratinocytes into the scratch is then observed over time. To assess the effect of Tcf3 overexpression on migration, we first performed the assay with primary keratinocytes isolated from tet-inducible Tcf3 (*K14-rtTA;TRE-mycTcf3*) transgenic mice[22], which express a tightly regulated, strongly doxycycline-inducible *Tcf3* transgene under the skin-specific keratin 14 promoter (Supplemental Fig. S2). We found that Tcf3-overexpressing keratinocytes showed an increase in cell migration of 60% compared with non-overexpressing controls (**$p<0.001$) (Fig. 1B, C), suggesting that Tcf3 can indeed functionally affect cell migration. Using *ex vivo* explant skin culture, we also found epithelial cells from Tcf3-induced skins migrated more than the control skins (**$p<0.001$) (Fig. 1D, E).

To determine whether the ability to promote cell migration is specific to Tcf3 or is a general characteristic of Lef/Tcf family members, we compared the effects of overexpression of all four Lef/Tcf members on cell migration. We transduced keratinocytes with GFP-tagged, tet-inducible lentiviral vectors[25] carrying myc-tagged

Tcf3, Tcf4, Lef1, or Tcf1 transgenes and enriched for transduced cells by fluorescent cell sorting. We then used doxycycline (Dox) to induce the expression of the Lef/Tcf genes 24 hours prior to performing the migration assay. All four Lef/Tcf members were expressed at similar levels upon Dox treatment (Supplemental Fig. S3A). Of the four Lef/Tcf members, only Tcf3 and Tcf4 promoted cell migration (**$p<0.001$) (Supplemental Fig. S3B, C). It is interesting to note that although Tcf4 is not induced at the wound edge *in vivo*, it does share the ability of Tcf3 to promote cell migration in this assay.

Tcf3 overexpression in epidermal cells promotes wound healing *in vivo*

Since overexpression of Tcf3 promotes cell migration *in vitro*, we wanted to determine whether Tcf3 expression could promote wound healing *in vivo*. We created full-thickness, 1 cm x 1 cm wounds on the dorsal skin of tet-inducible Tcf3 (*K14-rtTA;TRE-mycTcf3*) (n=5) or control (*K14-rtTA* or *TRE-mycTcf3*) (n=5) mice that had been maintained on a doxycycline-containing diet. We then measured the surface area of the wounds 6 and 10 days after wounding. We saw that wound closure was significantly accelerated in Tcf3-induced mice relative to controls (*$p<0.05$) (Fig. 2A, B). Accelerated wound repair was further confirmed by H&E staining of wound sections, which revealed much faster re-epithelialization in Tcf3-induced mice than controls (*$p<0.05$) (Fig. 2C, D). Expression of the *Tcf3* transgene was verified by immunofluorescent staining for Tcf3 (Supplemental Fig. S4A). Overexpression of Tcf3 did not lead to an increase in Ki67 staining at the wound edge (Supplemental Fig. S4B), suggesting that accelerated wound closure is mainly due to enhanced cell migration and not proliferation. Together with our previous finding that the loss of Tcf3 and Tcf4 causes defective wound repair[23], our current finding that Tcf3 overexpression is sufficient to promote wound healing strongly suggests a critical role for Tcf3 in normal wound repair *in vivo*.

Tcf3 is induced at the wound edge in response to Stat3 signaling

Next, we sought to identify factors that regulate Tcf3 expression in response to wounding. We identified three evolutionarily conserved Stat3 binding sites in the *Tcf3* promoter (Supplemental Fig. S5), suggesting that Stat3 could potentially activate Tcf3 transcription. Stat3 is one of seven members of the STAT (Signal Transducer and Activator of Transcription) family of transcription factors, which remain latent in the cytoplasm at baseline. Upon activation by phosphorylation on its tyrosine residue 705, Stat3 dimerizes and translocates into the nucleus, where it binds to conserved consensus sites on target genes and activates their transcription[26]. The role of Stat3 in promoting cell migration has been reported in numerous cases[2,27], but the genes directly targeted by Stat3 to regulate cell migration are still largely unknown.

Given that Stat3 is induced at the skin wound edge and that its ablation has been shown to impair wound repair[2], we next examined whether Stat3 regulates Tcf3 expression in response to wounding. As expected, we found activated Stat3 at the wound edge, mirroring the pattern of Tcf3 induction (Fig. 3A, B). In contrast, in *Stat3$^{fl/fl}$;K14-Cre* (*Stat3* cKO) mice, where epidermal Stat3 is conditionally ablated[28] by the epidermis-specific *keratin 14 Cre* driver[29], Tcf3 failed to be induced at the skin wound edge (Fig. 3C, D). We obtained similar results by *in situ* hybridization for Tcf3 mRNA (Fig. 3E, F). Thus, these data suggest that Stat3 is necessary for Tcf3 upregulation during the wound response.

We next tested Stat3-mediated *Tcf3* promoter activation by luciferase reporter assays, using a 5 kb *Tcf3* promoter fragment cloned from genomic DNA. We found that constitutively activated Stat3 (Stat3C) induced reporter expression from the *Tcf3* promoter ; activation of the reporter was abolished by mutation of the Stat3 binding sites (*$p<0.05$) (Fig. 3G, H). *Lef1* and *Tcf1* do not contain conserved Stat3 binding sites in their promoters while *Tcf4* contains one conserved Stat3 binding site. However, Stat3C

did not induce reporter expression from the 5 kb *Tcf4* promoter in the luciferase reporter assay (Supplemental Fig. S6).

To determine whether endogenous Stat3 directly binds to the *Tcf3* promoter *in vivo*, we used antibodies against Stat3 to perform chromatin immunoprecipitation (ChIP) on chromatin lysates from hair follicle cells. We detected endogenous Stat3 bound to the *Tcf3* promoter in regions containing conserved Stat3 binding sites (*$p<0.05$), but not in control regions that lack Stat3 binding sites (Fig. 3I). These results suggest that Stat3 directly binds and activates the *Tcf3* promoter.

Although Stat3 activates the *Tcf3* promoter *in vitro* and binds to the endogenous *Tcf3* promoter *in vivo*, overexpression of constitutively activated Stat3 (Stat3C) in the epidermis was not sufficient to induce expression of Tcf3 (Supplemental Fig. S7A, S7B). Furthermore, ablation of Stat3 in the skin does not alter the expression pattern of Tcf3 during normal development and homeostasis, as Tcf3 is expressed at similar levels in Stat3-deficient skin compared to wild-type skin (Supplemental Fig. S7C, S7D). Thus, although it is required for upregulation of Tcf3 in response to wounding, Stat3 activation alone is insufficient to activate Tcf3 expression.

Tcf3 overexpression rescues defective migration in Stat3-deficient cells

Previous reports have shown that ablation of epidermal Stat3 impairs cutaneous wound repair *in vivo* and cell migration *in vitro*[2]. Given our observations that Stat3 upregulates expression of Tcf3 at the skin wound edge and that Tcf3 promotes cell migration, the promotion of cell migration by Stat3 might be dependent on its induction of Tcf3. To address this, we next determined whether Tcf3 overexpression could rescue the cell migration defect caused by deficiency of Stat3. We cultured primary keratinocytes from *Stat3*$^{fl/fl}$*;K14-Cre (Stat3* cKO) mice[28], transduced them with GFP-tagged lentiviral vectors expressing tet-inducible Tcf3, and enriched them by fluorescent cell sorting. We then

treated the cells with Dox to induce expression of Tcf3 just prior to the migration assay. As expected, *Stat3* cKO keratinocytes showed impaired cell migration (**p<0.001). Importantly, this defect was reversed by Tcf3 overexpression (**p<0.001) (Fig. 4A, B). The observation that forced expression of Tcf3 can rescue defective migration in Stat3-deficient keratinocytes strongly suggests that Tcf3 is a key downstream effector of Stat3 in this process.

Tcf3 promotes cell migration non-cell-autonomously and independently of β-catenin

In light of the important role of Tcf3 in cell migration and wound healing, we sought to identify the mechanism by which Tcf3 affect this process. Since Tcf3 can function as both a β-catenin-dependent transcriptional activator and a β-catenin-independent repressor, we first tested which of these functions is necessary in cell migration. We transduced keratinocytes with GFP-tagged, tet-inducible lentiviral vectors carrying either myc-tagged wild-type Tcf3 or one of two Tcf3 deletion mutants: Tcf3ΔN, which does not bind to β-catenin and therefore cannot activate Wnt target genes; and Tcf3ΔG, which cannot bind Groucho/TLE-family corepressors and thus loses repressor function[20]. After enrichment by fluorescent cell sorting, the transduced cells were treated with Dox to induce the expression of wild-type or mutant Tcf3 (Fig. 5A; Supplemental Fig. S8A), and then subjected to the *in vitro* wounding assay. We found that overexpressing Tcf3ΔN promoted cell migration to a similar extent as wild-type Tcf3 (**p<0.001), while overexpressing Tcf3ΔG produced no significant effect on migration (Fig. 5B, C). The observation that Tcf3's pro-migratory effect requires its Groucho-interacting domain, but not its β-catenin-interacting domain, suggests that Tcf3 promotes cell migration by interacting with Groucho/TLE family members as a corepressor.

We next determined whether Tcf3 promotes cell migration cell-autonomously or by paracrine effects on neighboring cells. We cultured tet-inducible Tcf3 keratinocytes (*K14-rtTA;TRE-mycTcf3*) or single-transgenic controls (*K14-rtTA*) in the presence or absence of Dox and collected their conditioned media (CM). We then tested the ability of the CM to influence migration of wild-type keratinocytes. Cells that were incubated with CM from Tcf3-overexpressing cells displayed enhanced migration compared with cells incubated with control CM (**p<0.001). This suggests that Tcf3-induced cells produce secreted factors that affect the migration of wild type cells (Fig. 5D, E) and implies that Tcf3 promotes cell migration non-cell-autonomously.

Moreover, we found that CM from Tcf3ΔN-, but not Tcf3ΔG-overexpressing cells promoted cell migration (**p<00.1), confirming that indeed Tcf3 promotes cell migration independently of β-catenin and non-cell autonomously (Supplemental Fig. S8B).

Since Tcf3 promotes cell migration non-cell autonomously, we wanted to determine whether Tcf3 also non-cell autonomously promotes wound healing. After creating full thickness wounds of $1cm^2$ on the dorsal skin of wild-type mice, we applied CM from Tcf3-overexpressing cells (Tcf3-CM) or control cells onto the wound sites (n=5 each group). We found that daily application of Tcf3-CM onto the wound sites significantly accelerated wound closure (*p<0.05) (Fig. 6A, B).

Lipocalin 2 is the critical key secreted mediator of Tcf3-induced wound healing

Since Tcf3 promotes cell migration and wound healing in a non-cell autonomous manner, we sought to identify the secreted factors involved in this process. We searched previously compiled microarray data for genes encoding extracellular proteins that were upregulated upon Tcf3 overexpression[22]. Of the potential candidates, we verified that lipocalin 2 (Lcn2) expression is increased in response to Tcf3

overexpression in both cultured keratinocytes (Fig. 6C and Supplemental Fig. S9A,B) and *in vivo* in skin (Supplemental Fig. S9C). We also found that Lcn2 expression is induced at the wound edge (Supplemental Fig. S9D).

Lcn2 (also known as NGAL, 24p3, uterocalin, or siderocalin) is an acute-phase protein expressed in certain tissues in response to injury and inflammation[30]. It is also overexpressed in many types of cancer and is implicated in metastasis in breast cancer[31-33]. Moreover, it is involved in promoting cell motility in both neurons and cancer cells[33-36]. To determine whether Tcf3 promotes cell migration and wound healing through upregulation of Lcn2, we incubated the CM collected from Tcf3 overexpressing cells (Tcf3-CM) with antibodies against Lcn2 and evaluated how the inhibition of Lcn2 affects cell migration and wound healing. We found that immunodepletion of Lcn2 from Tcf3-CM reversed the pro-migratory effect *in vitro* (**$p<0.001$) (Fig. 6D) and its pro-wound closure effect *in vivo* (*$p<0.05$) (Fig. 6E and Supplemental Fig. S10). A similar loss of efficacy was observed following Lcn2 immunodepletion in the *ex vivo* explant culture system (*$p<0.05$) (Supplemental Fig. S11). Together these results suggest that Tcf3 promotes cell migration and wound healing through upregulation of the secreted factor Lcn2. Since our data suggest that the pro-migratory effects of Tcf3 are dependent on its transcriptional repressor function, the induction of Lcn2 due to Tcf3 overexpression is most likely to be an indirect effect.

To determine whether Lcn2 alone is sufficient to promote epidermal cell migration, we tested the effect of CM collected from Lcn2-overexpressing cells (Lcn2-CM) on cell migration. We found that keratinocytes that were incubated in Lcn2-CM migrated more than keratinocytes incubated with control CM (**$p<0.001$) (Fig. 6F). To determine whether Lcn2 itself can promote wound healing *in vivo*, we topically applied Lcn2-CM onto full-thickness wounds and evaluated its effect on the wound repair process. We found that the application of Lcn2-CM (n=4) accelerated wound closure significantly

(*p<0.05) more than the application of control CM (n=4) (Fig. 6G, H). Similarly, the application of recombinant Lcn2 protein onto wounds also substantially accelerated wound closure (*p<0.05) (Supplemental Fig. S12). Since overexpression of Lcn2 does not promote proliferation *in vitro* (Supplemental Fig. S9E), these data suggest that Lcn2 promotes wound healing by promoting cell migration.

To determine whether Lcn2 is essential in the wound repair process, we immunodepleted Lcn2 by topically applying anti-Lcn2 (n=8) or isotype control antibodies (n=8) onto full-thickness wounds in *nude* mice. Wounds that were treated with Lcn2 blocking antibodies repaired less efficiently than the wounds that were treated with IgG control (*p<0.05) (Fig. 7A, B). These data strongly suggest that Lcn2 is required for wound repair.

Exogenous Lcn2 rescues defective cell migration and wound healing in Stat3-deficient skin

Since Tcf3 overexpression can rescue defective cell migration in Stat3-deficient keratinocytes and Lcn2 is the key mediator of the Tcf3-induced promigratory effect, we sought to determine whether inhibition of Lcn2 could compromise the Tcf3-mediated rescue of Stat3-deficient keratinocytes. We first transduced primary keratinocytes from *Stat3*$^{fl/fl}$*;K14-Cre (Stat3* cKO) mice with a GFP-tagged lentiviral vector expressing tet-inducible Tcf3 or an empty vector control. After enriching them by fluorescent cell sorting, we then treated the cells with Dox to induce expression of Tcf3 prior to the migration assay. At the start of the migration assay we added Lcn2 blocking antibodies or isotype control antibodies to the keratinocytes and then quantified the migrated distance after 48hrs. As in our previous experiments, Stat3-deficient keratinocytes migrated less than the control (*K14-cre*;*Stat3*$^{+/fl}$) keratinocytes and overexpression of Tcf3 reversed this migration defect. However, when Lcn2 was depleted, overexpression

of Tcf3 could no longer rescue the defective migration in Stat3-deficient keratinocytes (**p<0.001) (Fig. 7C, Supplemental Fig. S13).

We next examined whether Lcn2 expression could rescue the defective wound repair process in Stat3-deficient skin. We created full-thickness wounds on *Stat3* cKO (n=11) or control mice (n=13) and applied recombinant Lcn2 protein or vehicle control onto the wound beds. As expected, *Stat3* cKO skin showed defective wound repair (**p<0.001). Importantly, the application of recombinant Lcn2 rescued the defective wound healing in *Stat3* cKO skin (*p<0.05) (Fig. 7D, E). These data suggest that Stat3's role in cell migration and wound healing is mediated by Lcn2 via Tcf3.

DISCUSSION

To understand and enhance the wound repair process, it is essential to understand the molecular mechanisms underlying the steps contributing to wound repair. Stat3 is one of the few known transcription factors that have been implicated in cell migration and re-epithelialization during wound repair. Conditional ablation of Stat3 in the mammalian epidermis impairs cutaneous wound healing *in vivo* and epidermal cell migration *in vitro*[2]. Stat3 deficiency causes cell migration defects during gastrulation in zebrafish[27]. Mice carrying null alleles of Stat3 also die during early gastrulation[37], suggesting that Stat3 plays a similar role in cell migration during mouse development. In addition, aberrant Stat3 activity promotes tumor invasion and metastasis in various cancers[38-42]. Despite the evident role of Stat3 in cell migration, the downstream genes targeted by Stat3 to regulate cell migration are still largely unknown.

Our demonstration that Stat3 directly upregulates Tcf3 expression during wounding and that Stat3 can directly activate Tcf3 transcription provides the first direct link between the Stat3 and Tcf3 transcriptional networks, both of which are crucial for tissue homeostasis. More importantly, we show that Tcf3 itself promotes cell migration and

that its forced expression rescues defective cell migration in Stat3-deficient cells. Our data not only uncover a novel role for Tcf3 in cell migration, they also suggest that Stat3 promotes cell migration through its upregulation of Tcf3.

Moreover, our findings that Tcf3 is induced in response to wounding and directly promotes wound healing demonstrate a crucial role for transcriptional regulation of Lef/Tcf factors in determining functional outcomes. This is in contrast with the traditional model in which Tcf activity is primarily regulated by the presence or absence of nuclear β-catenin. In addition, our finding that Tcf3 can promote cell migration without its β-catenin-interacting domain presents a novel β-catenin-independent role for Tcf3 and underlines the importance of Tcf3's ability to act as a transcriptional repressor.

It is interesting to note that overexpression a ΔNLef, a truncated Lef1 that lacks a β-catenin binding site, in the skin results in a delay of wound closure[43]. Because ΔNLef inhibits β-catenin signaling, it is thought that impaired Wnt signaling maybe the cause of the delay in wound healing. However, inhibition of Wnt signaling by overexpression of the Wnt inhibitor Dkk1 does not alter wound closure, instead affecting only hair follicle neogenesis[44]. This suggests that Wnt signaling is not crucial for the reepithelialization process. Consistent with the nonessential role of Wnt in epidermal wound repair, overexpression of Wnt (Wnt7a) does not affect wound closure[44]. It is therefore tempting to speculate that ΔNLef delays wound closure by a negative effect on Tcf3, possibly though direct competition with Tcf3 for target gene binding.

Finally, our novel observation that Tcf3 acts non-cell-autonomously via Lcn2 to promote migration and wound healing offers a new mechanism by which Tcf3 acts to shape the tissue microenvironment during wounding. We have shown that topical application of CM collected from Tcf3-overexpressing cells or Lcn2-overexpressing cells both enhance wound healing in mice. Blockade of Lcn2 impairs wound healing and

diminishes Tcf3-CM's ability to affect cell migration, suggesting that the secretion of Lcn2 is both necessary and sufficient to promote cell migration and wound healing in response to Tcf3.

Lcn2 is an acute phase protein, upregulated at sites of inflammation and injury[30,34,45]. It is an established biomarker for renal injury, and its levels are increased in serum of patients with psoriasis[46,47]. It is also expressed at a high level in a variety of tumors[48-51]. Lcn2's diverse roles range from being a bacteriostatic agent to a promoter of cell motility[52,53]. Lcn2's role in cell migration has been shown in several model systems. Ablation of Lcn2 results in impaired migration of astrocytes to injury sites in both mice and zebrafish[36,54]. Overexpression of Lcn2 *in vitro* increases cell motility and invasiveness of breast cancer cells[33,34]. Although Lcn2 can promote cell motility, the molecular mechanism underlying this function is not known. Overexpression of Lcn2 downregulates expression of E-cadherin and increases expression of mesenchymal markers, while downregulation of Lcn2 inhibits cell migration and the mesenchymal phenotype[34]. Based on this finding, it is conceivable that Lcn2 promotes cell migration by affecting cell adhesion via its downregulation of E-cadherin. However, how Lcn2 brings about the downregulation of E-cadherin is still unknown.

Furthermore, since Lcn2 binds to and stabilizes matrix metalloproteinase-9 (MMP9) [55], a proteinase that is important for cell migration and wound healing, it is also possible that Lcn2 promotes cell migration by increasing the activity of MMP-9. MMP-9 belongs to the MMP family of zinc-dependent endopeptidases that degrade components of the extracellular matrix, allowing cell migration to occur[56]. Mice with MMP-9 deficiency show delayed cell migration and wound repair[57].

Although it remains to be elucidated how Lcn2 promotes cell migration, our findings clearly demonstrate that Lcn2 has a crucial role in promoting epidermal cell migration and wound healing in skin. We show that the application of Lcn2 to the wound sites

substantially accelerates wound healing while the application of antibodies against Lcn2 significantly delays wound healing. Importantly, the application of Lcn2 rescues defective wound healing in Stat3-deficient skin, suggesting that Stat3 acts through Tcf3's downstream effector Lcn2.

Although our data clearly show that Tcf3 overexpression induces the expression of Lcn2 and promotes cell migration and wound healing, we still do not know how Tcf3 brings about the induction of Lcn2. Tcf3's promotion of cell migration is dependent on its interaction with the transcriptional repressor Groucho and not with the activator β-catenin, suggesting that Tcf3 acts as a repressor in its role in cell migration. Hence, it is likely that Tcf3 represses repressor(s) of Lcn2 expression, which consequently leads to the induction of Lcn2. We are currently seeking to identify the regulator(s) of Lcn2 that Tcf3 affects that impact cell migration and wound healing.

In conclusion, we identify a novel role for Tcf3 and Lcn2 in epidermal cell migration and skin wound repair. Lcn2 is already implicated in innate immune response to bacterial invasion and cell motility in neurons and cancer cells[33-36,52,53]. Our findings identify a new role for Lcn2 in epidermal cell migration and skin wound healing and also provide a potential target for development of new treatments for defective wound repair.

METHODS

Mice

Tet-inducible Tcf3 mice were generated by crossing *K14-rtTA* with *TRE-Tcf3* [22]. Intercrosses between the *Stat3*$^{fl/fl}$ line[28] and *K14-Cre* (Jackson Laboratory) were done to yield *Stat3* cKO mice. Intercrosses between the *Tcf3*$^{fl/fl}$ line[23] and *K14-Cre* yielded *Tcf3* cKO mice.

Tet-inducible Stat3C transgenic mice were generated by crossing *K14-rtTA* with *TRE-Stat3C*. The *XhoI* and *DrdI* fragment of *pTRE-Stat3C* was microinjected into pronuclei of FVB/N embryos to generate the *TRE-Stat3C* transgenic line.

In vivo wound closure assay

For wounding experiments, 8- to 10-week-old *Stat3* cKO (*Stat3*$^{fl/fl}$*;K14-Cre*) or control (*Stat3*$^{fl/f}$) mice were anesthetized with intraperitoneal administration of ketamine/xylazine and full-thickness wounds were made on the mid dorsal skin with 4-mm disposable biopsy punches. Skins were harvested and embedded in OCT (Tissue-Tek) 3, 5, or 7 days post wounding.

To evaluate the effect of Tcf3 expression on wounds repair, full thickness wounds of 1 cm^2 were created on the dorsal skins of Tcf3 inducible (*K14-rtTA;TRE-mycTcf3)* or control (*K14-rtTA* or *TRE-mycTcf3*) mice which had been maintained on doxycycline (200mg/kg) containing chow (Bio-Serv) for 6 months starting at 8 weeks of age. Skins were harvested and embedded in OCT 6 or 10 days post-wounding.

To evaluate the effect of conditioned media (CM) from Tcf3- or Lcn2-overexpressing cells on wound closure, full thickness wounds of 1cm^2 were created on the dorsal skins of 8-10 week old ICR mice. 200 µl of CM was topically applied onto the wound sites and the surface areas of the wounds were measured. Each wound was covered with Tegaderm film and a self-adherent wrap (Coban) to prevent leakage, desiccation and infection.

CM was generated by feeding 80~90% confluent keratinocytes in 15-cm tissue culture plates with 18 ml/plate serum-free MCDB153 medium and incubating for 48 h. The CM was concentrated 10-fold by using Amicon centrifugal filter units with a 10-kDa cut-off (Millipore) following the manufacturer's instructions. The concentrated CM was mixed with carboxymethylcellulose solution (final concentration, 3% w/v) before being topically

applied onto the wound bed. To evaluate the effect of recombinant Lcn2 on wound closure, 200µl of Lcn2 (R&D Systems), dissolved at 1µg/ml in PBS + 3% carboxymethylcellulose was applied onto the wound bed and wound closure was evaluated as described above. To evaluate the depletion of Lcn2 on wound healing, 200µl of 3µg/ml anti-Lcn2 (R&D Systems) or goat IgG in PBS+3% carboxymethylcellulose were applied every other day for 11 days to $1cm^2$ wounds that were created on *nude* mice. To evaluate whether recombinant Lcn2 can rescue defective wounding healing in *Stat3* cKO mice, $1cm^2$ wounds were created on dorsal skins of *Stat3* cKO or littermate controls that were waxed for 2 weeks prior to wounding. 200µl of 2µg/ml EGF (Invitrogen) with or without recombinant 2µg/ml of Lcn2 in PBS +3% carboxymethylcellulose were applied to the wound beds every other for 11 days. Wound closure was evaluated as described above.

All mice were maintained in the AALAC-accredited animal facility at Baylor College of Medicine and were used according to protocols that were approved by the Baylor College of Medicine institutional care and use committee.

Ex vivo skin explant outgrowth assay

Ex vivo explant culture of 2~4 d old mouse skin was carried out as previously described[58,59]. Circular skin biopsies were obtained from dorsal skin of 2-d-old mice using 4-mm punches (Sklar) and plated with 0.3-ml medium in 24-well plates (BD Biosciences). After overnight incubation at 37°C, 7.5% CO2, explants were submerged in media with or without Dox (1 µg/ml) and grown for another 8 d before fixing (4% PFA for 10 min; 100% methanol for 10 min at -20°C). Medium was changed every 2–3 d. In cases of Mitomycin C treatment, skin explants were treated with 8 µg/ml Mitomycin C (Roche) 48 h post Dox treatment. After Mitomycin C treatment, cultures were washed three times with PBS and refed with fresh media. Keratinocytes in the cellular outgrowth

of explants were identified by immunostaining for Keratin 17 and by morphological appearance. Images of the cellular outgrowth from each explant were taken, and the proximal distance extending between the explant biopsy and the distal edge of the cellular migration was measured using NIH ImageJ software (http://rsb.info.nih.gov/ij/). Measuring the surface area covered by the keratin 17-positive outgrowth yielded similar findings.

Plasmid constructs

Gateway entry vectors for the *Lef/Tcf* genes of interest were generated as follows: The myc-tagged *Tcf3* wild-type and mutant alleles[20] were PCR-amplified from their respective vectors with the addition of *Eco*RI and *Xho*I sites with primers myctag_EcoRI_fw and Tcf3ΔC_XhoI_rv2 (for *Tcf3ΔC*) or Tcf3_XhoI_rv (for the others). The PCR was conducted using Phusion DNA polymerase (New England Biolabs, Ipswich, MA). The resulting PCR products were then subcloned into pENTR 1A (Life Technologies, Carlsbad, CA). Myc-tagged *Tcf4* was subcloned from K14-mycmTcf4[23] into pENTR 1A by *Bam*HI/*Not*I digest. Myc-tagged *Lef1* was subcloned from K14-mycmLef1[60] into pENTR 1A by *Eco*RI/*Xba*I digest. To clone myc-tagged *Tcf1*, total RNA was TRIzol-purified from adult C57BL/6 mouse splenocytes and reverse-transcribed into cDNA using SuperScript III reverse transcriptase (Life Technologies, Carlsbad, CA) with oligo$(dT)_{20}$ primers. The full-length *Tcf1* ORF (from NM_009331) was PCR-amplified, with the addition of *Eco*RI and *Not*I sites and a myc tag, using the primers mTcf1_myc_Eco_fw and mTcf1_Not_rv. The PCR was conducted using Herculase II polymerase (Agilent Technologies, Santa Clara, CA). The resulting PCR product was digested and subcloned directly into *Eco*RI/*Not*I-digested pENTR 1A. A negative-control entry vector was generated by digesting pENTR 1A with *Eco*RI (to release the ccdB suicide gene) and recircularizing it. To generate Tet-inducible lentivirus constructs, the

Gateway entry vectors were recombined into pINDUCER21[25] using LR Clonase II (Life Technologies, Carlsbad, CA) according to the manufacturer's instructions.

Tcf3pro-*luc* constructs were generated by PCR from mouse embryonic stem cell genomic DNA. 4884bp of the proximal Tcf3 promoter was amplified with primers to introduce an *Mlu*I site at the 5' end and an *Xho*I site at the 3' end. The fragment was then subcloned into the pGL3-basic vector (Promega). Site-directed point mutation of Tcf3 promoter for Stat3 binding sites was made as described[61].

pTRE-Stat3C was engineered as follows: the *β-globin* intron was subcloned from the *K14* cassette vector (Elaine Fuchs lab) into the *SacII* site of *pTRE2* (Clontech) to form the vector *pTRE2I*. The *Stat3C-Flag* ORF from the *pBabe-Stat3C* expression vector (a gift from Dr. Jacqueline Bromberg of Memorial Sloan-Kettering Cancer Institute) was digested with *BamHI,* then ligated into the *BamHI* site of *pTRE2I*.

All plasmids were verified by restriction digest and sequencing before use. All cloning primers are listed in Supplementary Table 1.

Lentivirus production

293T cells were cultured in IMDM containing 10% FBS, 2 mM supplemental L-glutamine, and pen/strep. To produce lentivirus particles, cells were plated at 4 x 10^6 cells per 10 cm plate. The following morning, they were transfected with 7 µg pINDUCER vector and 750 ng each of pHDM-Hgpm2, pRc/CMV-RaII, pHDM-tat1b, and pHDM-VSV-G with 30 µL of TransIT-293 transfection reagent (Mirus Bio) per 10 cm plate. 24 hours after transfection, media was changed and volume reduced to 6 mL per 10 cm plate. Virus-containing supernatants were collected at 48 and 72 hours post-transfection, pooled, and concentrated by ultracentrifugation at 85,000 x g for two hours. Virus particles were resuspended in a small amount of keratinocyte growth media, separated into aliquots, and stored at -80°C until use. Virus preps were titered by infection of 293T cells with 10-

fold serial dilutions of lentivirus followed by flow cytometric analysis for GFP positivity. Titers (in transduction units per microliter) were calculated using the formula [(fraction GFP positive)(number of cells at time of infection)] / [(dilution factor)(volume of viral inoculum)].

Keratinocyte culturing and lentiviral infection

Primary keratinocytes were isolated as described[22]. Primary keratinocytes were cultured on J2 fibroblasts treated with Mitomycin C (Roche) for 3 passages before being cultured without feeder cells.

For lentiviral infections, keratinocytes were plated at 1 x 10^5 cells per well in 6-well tissue culture plates. The following day, one or two representative wells were trypsinized and counted. Lentivirus preps were thawed and diluted in keratinocyte growth media containing 8 µg/mL Polybrene (Sigma-Aldrich, St. Louis, MO), to a final multiplicity of 5 transduction units per cell. Growth media was aspirated from the plated keratinocytes and replaced with diluted lentivirus (1 mL/well). The plates were incubated at 37°C for 15 minutes and then centrifuged at 1100 x g, 32°C, for 30 minutes. After centrifuging, the cells were washed with 3 mL/well PBS, refed with keratinocyte growth media, and returned to 37°C for growth. GFP expression was detectable 72 hours following infection.

For the cell proliferation assay, 2 x 10^4 cells were plated onto each well of a 24 well plate. Cells were trypsinized and counted in triplicates using a Beckman Z2 Coulter counter every 24 hours.

Flow Cytometry

After lentiviral transduction, cells were grown to confluence, and then sorted by flow cytometry. Cells were trypsinized, then resuspended in ice-cold sorting buffer (4%

calcium-free chelated FBS in PBS, ~200-300 μm per 10cm plate), and strained into 30 μm strainer-cap FACS tubes and kept on ice. Cells were isolated on a FACSAria II or IIu cell sorter (BD Biosciences), using the 100 μm nozzle at a sheath pressure of 20 psi. GFP positives (typically 60-80% of cells) were collected in chilled 15 mL catch tubes containing 6 mL of keratinocyte growth media. After collection, cells were pelleted, resuspended, counted, and replated for growth in keratinocyte growth media.

In vitro wounding assay

The *in vitro* wounding assay was performed as described[2,24] with some modifications. Keratinocytes were cultured in 6-well plates until reaching confluence. They then were starved in serum-free basal medium with or without doxycycline for 22 hr, followed by treatment with 10 μg/ml Mitomycin C for 2 hr. After creating a straight scratch with a pipet tip, the cells were washed three times with PBS to remove Mitomycin C and cell debris. For testing functions of various genes in cell migration, the cells were refed with serum-containing medium with or without doxycycline, and cell migration was stopped 14~16 hrs later by fixing with 3.8% PFA. Alternatively, in the rescue experiments, following starvation, Mitomycin C treatment and scratching, the cells were incubated in basal medium complemented with 10 ng/ml mouse recombinant EGF (Invitrogen, United States) with or without doxycycline. Immediately after a scratch was created, markings were made adjacent to the scratch as a reference for camera positioning. Photographs were taken at the initial and final time points using a phase-contrast microscope (Axiovert 40; Zeiss, Germany). By comparing the images from initial to final timepoints, the area filled by migrating cells was quantified with ImageJ analysis software (http://rsb.info.nih.gov/ij/). For each sample, over 30 non-overlapping fields were measured at each timepoint; and each experiment was repeated at least twice. Values represent the mean ± s.e.m. of migrated area beyond the edges of the scratch.

Luciferase reporter assay

pBabe-Stat3 and *pBabe-Stat3C* expression vectors were gifts from Dr. Jacqueline Bromberg (Memorial Sloan-Kettering Cancer Institute). For the reporter assay, keratinocytes were plated at density of 2 x 10^4 cells per well in a 24-well plate one day before transfection. The *Tcf3*pro-luc, *Tcf4*pro-luc and the Stat3 expression vector, along with the control vector *pRL-TK* were transfected using FuGENE 6 (Roche) according to the manufacturer's instructions. Luciferase reporter activity was measured using the Dual-Luciferase Reporter system 48 hours after transfection (Promega) with Firefly luciferase values normalized to *Renilla* luciferase values.

Real-time PCR

Total RNA was purified with the ZR RNA Miniprep kit (Zymo Research, Irvine, CA) and 1ug of each RNA sample was reverse transcribed with the Superscript III First-Strand Synthesis System (Life Technologies, Carlsbad, CA) using Oligo(dT) primers. PCR amplifications of genes of interest were performed using primers located in different exons or spanning intron-exon junctions to obtain amplicons less than 150 bp in length. Real-time PCR was performed with LightCycler DNA Master SYBR Green I reagents on a LightCycler 480 real-time PCR system (Roche, United States). Differences between samples and controls were calculated based on the $2^{-\Delta\Delta CP}$ method, using the Mrpl19 gene as an internal control. Primer sequences are listed in Supplemental Table 1.

Immunohistochemistry and immunofluorescence

For immunohistochemical detection, 5 µm paraffin sections were used; and endogenous biotin and peroxidase activity were blocked. The color was developed with DAB chromogen (ImmPACT DAB; VectorLabs, United States) and the sections were counterstained with hematoxylin.

Immunofluorescence analysis was performed as described[22]. 6~8 μm frozen backskin sections were fixed in 4% PFA. For blocking, the MOM kit (Vector Laboratories, Burlingame, CA) was used for mouse monoclonal antibodies, and the following blocking buffer for all other antibodies: 10% normal donkey serum, 2% BSA, 2% fish skin gelatin, 2% Triton X-100 in PBS. Primary antibodies were used at the following concentration: guinea pig anti-Tcf3 (1:200, lab-generated), goat anti-Tcf4 (1:100; Santa Cruz), rabbit anti-Tcf1 (1:50; Cell Signaling), rabbit anti-Lef1 (1:150; Cell Signaling), mouse anti-myc tag (1:500; Zymed), mouse anti-β-catenin (Sigma), mouse anti-Stat3 (1:300; Cell Signaling), pY705-Stat3 (1:100; Cell Signaling), rat anti-cd104 (1:200; BD Biosciences) goat anti-Lcn2 (1:150;R&D Systems). Antigens were visualized with FITC- or RRX-conjugated secondary Abs (Jackson Labs). All images were acquired with Zeiss Axioskop microscope.

Immunoblot and in situ hybridization

To analyze tet-inducible gene expression, 40 μg protein from the total cell lysate of lentivirus-transduced keratinocytes was resolved by SDS-PAGE. The separated proteins were then immunoblotted, probed with primary myc tag antibody (1:3000, Abcam), and detected by chemiluminescence (SuperSignal West Pico, Thermo Scientific).

The *in situ* hybridization was carried out as described previously[62]. 5-day post wounding back skins of 8-10 week-old wild-type and *Stat3* cKO mice were frozen side by side in Tissue-Tek OCT reagent, and cryo-sections (16 μm) were prepared. The sections were fixed in 4% formaldehyde in PBS and acetylated, followed by pre-hybridization. Probes used were DIG-labeled (Roche) sense and anti-sense transcripts of mouse cDNAs of *Tcf3* (NM_001079822, nucleotides 1-1030). After hybridization, sections were treated with RNase A and extensively washed. The DIG-label was detected by an anti-DIG Fab

(Roche) coupled to alkaline phosphatase using NBT/BCIP (Roche) according to the manufacturer's instructions. Sections were then counterstained with nuclear fast red (Vector Laboratories).

Chromatin immunoprecipitation

In vivo chromatin immunoprecipitation (ChIP) was performed according to a modification of a protocol from Upstate Biotechnology. Hair follicle cells were isolated from P4 mouse pups as described[62] and were treated with 1.42% formaldehyde in 4% FBS-PBS solution at room temperature for 15 min. Cross-linked DNA was sonicated to form fragments ranging from 200 to 500 bp in length. After preclearing, ChIP lysates were immunoprecipitated with rabbit anti-Stat3 (Cell Signaling), and rabbit IgG (Jackson Laboratory). Pulled-down DNA fragments were recovered with the Chelex-100-mediated purification method[63]. Conserved Stat3 sites identified by rVista analysis of 5′ upstream sequences were defined by the ECR Browser and Ensembl software. Stat3 sites were chosen for ChIP analysis based on the conservation and alignment between mouse, rat and human. qPCR was done with the LightCycler 480 system (Roche, United States) using the PerfeCTa SYBR Green FastMix kit (Quanta Biosci) and primers to produce amplicons less than 150 bp. Primer sequences are listed in Supplemental Table 1.

Statistical Analysis

Statistical analyses were performed using Microsoft Excel. The Student's t-Test function with a two-tailed distribution was used to calculate p values. Differences were regarded as statistically significant and as statistically highly significant if p values were <0.05, and $p < 0.001$, respectively.

Acknowledgments

We would like to thank Drs. Wei Li and Fred Tsen from University of Southern California, and Drs. Junji Takeda and Shigetoshi Sano from Osaka University Medical School for their advice on experimental methods. We also would like to thank Drs. H.A. Dierick, M. Rendl, B. Deneen and M. Goodell for their critical reading of the manuscript. This work was supported in part by research grants from the Dan L. Duncan Cancer Scholar Award, The Naman Family Fund for Basic Research and Caroline Wiess Law Fund for Molecular Medicine, the Curtis and Doris K. Hankamer Foundation, and R01-AR059122.

Author Contribution

Q.M, Y.N. and H.N. designed the experiments and analyzed the results. Q.M, A.K, Y.N. and T.M.S. performed the experiments. K.L.M. generated the tet-inducible lentiviral backbone construct in T.F.W.'s laboratory. J.M.H. generated all the Lef/Tcf-expressing lentiviral constructs. G.G. and D.L. performed mouse husbandry and genotyping. $Stat3^{fl/fl}$ mice were generated in V.P.'s laboratory. J.M.H. and H.N. wrote the manuscript.

Competing Financial Interests

The authors declare no competing financial interests.

REFERENCES

1 Martin, P. Wound healing--aiming for perfect skin regeneration. *Science* **276**, 75-81 (1997).

2 Sano, S. *et al.* Keratinocyte-specific ablation of Stat3 exhibits impaired skin remodeling, but does not affect skin morphogenesis. *EMBO J* **18**, 4657-4668, (1999).

3 Li, G. *et al.* c-Jun is essential for organization of the epidermal leading edge. *Dev Cell* **4**, 865-877 (2003).

4 Repertinger, S. K. *et al.* EGFR enhances early healing after cutaneous incisional wounding. *J Invest Dermatol* **123**, 982-989 (2004).

5 Tan, N. S. *et al.* The nuclear hormone receptor peroxisome proliferator-activated receptor beta/delta potentiates cell chemotactism, polarization, and migration. *Mol Cell Biol* **27**, 7161-7175 (2007).

6 Chmielowiec, J. *et al.* c-Met is essential for wound healing in the skin. *J Cell Biol* **177**, 151-162 (2007).

7 Michalik, L. *et al.* Impaired skin wound healing in peroxisome proliferator-activated receptor (PPAR)alpha and PPARbeta mutant mice. *J Cell Biol* **154**, 799-814 (2001).

8 MacDonald, B. T., Tamai, K. & He, X. Wnt/beta-catenin signaling: components, mechanisms, and diseases. *Dev Cell* **17**, 9-26 (2009).

9 Arce, L., Yokoyama, N. N. & Waterman, M. L. Diversity of LEF/TCF action in development and disease. *Oncogene* **25**, 7492-7504 (2006).

10 Kim, C. H. *et al.* Repressor activity of Headless/Tcf3 is essential for vertebrate head formation. *Nature* **407**, 913-916 (2000).

11 Pereira, L., Yi, F. & Merrill, B. J. Repression of Nanog gene transcription by Tcf3 limits embryonic stem cell self-renewal. *Mol Cell Biol* **26**, 7479-7491 (2006).

12 Wray, J. *et al.* Inhibition of glycogen synthase kinase-3 alleviates Tcf3 repression of the pluripotency network and increases embryonic stem cell resistance to differentiation. *Nat Cell Biol* **13**, 838-845.

13 Yi, F. *et al.* Opposing effects of Tcf3 and Tcf1 control Wnt stimulation of embryonic stem cell self-renewal. *Nat Cell Biol* **13**, 762-770.

14 Gribble, S. L., Kim, H. S., Bonner, J., Wang, X. & Dorsky, R. I. Tcf3 inhibits spinal cord neurogenesis by regulating sox4a expression. *Development* **136**, 781-789 (2009).

15 Cole, M. F., Johnstone, S. E., Newman, J. J., Kagey, M. H. & Young, R. A. Tcf3 is an integral component of the core regulatory circuitry of embryonic stem cells. *Genes Dev* **22**, 746-755 (2008).

16 Ivanova, N. B. *et al.* A stem cell molecular signature. *Science* **298**, 601-604 (2002).

17 Chambers, S. M. *et al.* Hematopoietic fingerprints: an expression database of stem cells and their progeny. *Cell Stem Cell* **1**, 578-591 (2007).

18 Lie, D. C. *et al.* Wnt signalling regulates adult hippocampal neurogenesis. *Nature* **437**, 1370-1375 (2005).

19 DasGupta, R. & Fuchs, E. Multiple roles for activated LEF/TCF transcription complexes during hair follicle development and differentiation. *Development* **126**, 4557-4568 (1999).
20 Merrill, B. J., Gat, U., DasGupta, R. & Fuchs, E. Tcf3 and Lef1 regulate lineage differentiation of multipotent stem cells in skin. *Genes Dev* **15**, 1688-1705 (2001).
21 Merrill, B. J. *et al.* Tcf3: a transcriptional regulator of axis induction in the early embryo. *Development* **131**, 263-274 (2004).
22 Nguyen, H., Rendl, M. & Fuchs, E. Tcf3 governs stem cell features and represses cell fate determination in skin. *Cell* **127**, 171-183 (2006).
23 Nguyen, H. *et al.* Tcf3 and Tcf4 are essential for long-term homeostasis of skin epithelia. *Nat Genet*, (2009).
24 Liang, C. C., Park, A. Y. & Guan, J. L. In vitro scratch assay: a convenient and inexpensive method for analysis of cell migration in vitro. *Nat Protoc* **2**, 329-333, (2007).
25 Meerbrey, K. L. *et al.* The pINDUCER lentiviral toolkit for inducible RNA interference in vitro and in vivo. *Proc Natl Acad Sci U S A* **108**, 3665-3670.
26 Darnell, J. E., Jr. STATs and gene regulation. *Science* **277**, 1630-1635 (1997).
27 Yamashita, S. *et al.* Stat3 Controls Cell Movements during Zebrafish Gastrulation. *Dev Cell* **2**, 363-375, doi:S1534580702001260 [pii] (2002).
28 Alonzi, T. *et al.* Essential role of STAT3 in the control of the acute-phase response as revealed by inducible gene inactivation [correction of activation] in the liver. *Mol Cell Biol* **21**, 1621-1632, doi:10.1128/MCB.21.5.1621-1632.2001 (2001).
29 Dassule, H. R., Lewis, P., Bei, M., Maas, R. & McMahon, A. P. Sonic hedgehog regulates growth and morphogenesis of the tooth. *Development* **127**, 4775-4785 (2000).
30 Li, C. & Chan, Y. R. Lipocalin 2 regulation and its complex role in inflammation and cancer. *Cytokine* **56**, 435-441(.2011)
31 Rodvold, J. J., Mahadevan, N. R. & Zanetti, M. Lipocalin 2 in cancer: when good immunity goes bad. *Cancer Lett* **316**, 132-138(2011)
32 Shi, H. *et al.* Lipocalin 2 promotes lung metastasis of murine breast cancer cells. *J Exp Clin Cancer Res* **27**, 83 (2008).
33 Leng, X. *et al.* Inhibition of lipocalin 2 impairs breast tumorigenesis and metastasis. *Cancer Res* **69**, 8579-8584 (2009).
34 Yang, J. *et al.* Lipocalin 2 promotes breast cancer progression. *Proc Natl Acad Sci U S A* **106**, 3913-3918 (2009).
35 Lin, H. H. *et al.* Lipocalin-2-induced cytokine production enhances endometrial carcinoma cell survival and migration. *Int J Biol Sci* **7**, 74-86.
36 Kim, H. *et al.* Modulation of glial and neuronal migration by lipocalin-2 in zebrafish. *Immune Netw* **11**, 342-347, doi:10.4110/in.2011.11.6.342.
37 Takeda, K. *et al.* Targeted disruption of the mouse Stat3 gene leads to early embryonic lethality. *Proc Natl Acad Sci U S A* **94**, 3801-3804 (1997).
38 Wei, D. *et al.* Stat3 activation regulates the expression of vascular endothelial growth factor and human pancreatic cancer angiogenesis and metastasis. *Oncogene* **22**, 319-329 (2003).

39 Silver, D. L., Naora, H., Liu, J., Cheng, W. & Montell, D. J. Activated signal transducer and activator of transcription (STAT) 3: localization in focal adhesions and function in ovarian cancer cell motility. *Cancer Res* **64**, 3550-3558, doi:10.1158/0008-5472.CAN-03-3959 (2004).
40 Xie, T. X. *et al.* Stat3 activation regulates the expression of matrix metalloproteinase-2 and tumor invasion and metastasis. *Oncogene* **23**, 3550-3560 (2004).
41 Itoh, M. *et al.* Requirement of STAT3 activation for maximal collagenase-1 (MMP-1) induction by epidermal growth factor and malignant characteristics in T24 bladder cancer cells. *Oncogene* **25**, 1195-1204 (2006).
42 Barbieri, I. *et al.* Constitutively active Stat3 enhances neu-mediated migration and metastasis in mammary tumors via upregulation of Cten. *Cancer Res* **70**, 2558-2567.
43 Niemann, C., Owens, D. M., Hulsken, J., Birchmeier, W. & Watt, F. M. Expression of DeltaNLef1 in mouse epidermis results in differentiation of hair follicles into squamous epidermal cysts and formation of skin tumours. *Development* **129**, 95-109 (2002).
44 Ito, M. *et al.* Wnt-dependent de novo hair follicle regeneration in adult mouse skin after wounding. *Nature* **447**, 316-320 (2007).
45 Liu, Q. & Nilsen-Hamilton, M. Identification of a new acute phase protein. *J Biol Chem* **270**, 22565-22570 (1995).
46 Bolignano, D. *et al.* Urinary neutrophil gelatinase-associated lipocalin (NGAL) is associated with severity of renal disease in proteinuric patients. *Nephrol Dial Transplant* **23**, 414-416 (2008).
47 Kamata, M. *et al.* Serum lipocalin-2 levels are increased in patients with psoriasis. *Clin Exp Dermatol* **37**, 296-299, doi:10.1111/j.1365-2230.2011.04265.x.
48 Nielsen, B. S. *et al.* Induction of NGAL synthesis in epithelial cells of human colorectal neoplasia and inflammatory bowel diseases. *Gut* **38**, 414-420 (1996).
49 Lim, R. *et al.* Neutrophil gelatinase-associated lipocalin (NGAL) an early-screening biomarker for ovarian cancer: NGAL is associated with epidermal growth factor-induced epithelio-mesenchymal transition. *Int J Cancer* **120**, 2426-2434, doi:10.1002/ijc.22352 (2007).
50 Roy, R. *et al.* Tumor-specific urinary matrix metalloproteinase fingerprinting: identification of high molecular weight urinary matrix metalloproteinase species. *Clin Cancer Res* **14**, 6610-6617, doi:14/20/6610 (2008).
51 Bauer, M. *et al.* Heterogeneity of gene expression in stromal fibroblasts of human breast carcinomas and normal breast. *Oncogene* **29**, 1732-1740 (2009)
52 Flo, T. H. *et al.* Lipocalin 2 mediates an innate immune response to bacterial infection by sequestrating iron. *Nature* **432**, 917-921 (2004).
53 Berger, T. *et al.* Lipocalin 2-deficient mice exhibit increased sensitivity to Escherichia coli infection but not to ischemia-reperfusion injury. *Proc Natl Acad Sci U S A* **103**, 1834-1839 (2006).
54 Lee, S. *et al.* Lipocalin-2 Is a chemokine inducer in the central nervous system: role of chemokine ligand 10 (CXCL10) in lipocalin-2-induced cell migration. *J Biol Chem* **286**, 43855-43870.

55 Yan, L., Borregaard, N., Kjeldsen, L. & Moses, M. A. The high molecular weight urinary matrix metalloproteinase (MMP) activity is a complex of gelatinase B/MMP-9 and neutrophil gelatinase-associated lipocalin (NGAL). Modulation of MMP-9 activity by NGAL. *J Biol Chem* **276**, 37258-37265 (2001).
56 Steffensen, B., Hakkinen, L. & Larjava, H. Proteolytic events of wound-healing--coordinated interactions among matrix metalloproteinases (MMPs), integrins, and extracellular matrix molecules. *Crit Rev Oral Biol Med* **12**, 373-398 (2001).
57 Kyriakides, T. R. *et al.* Mice that lack matrix metalloproteinase-9 display delayed wound healing associated with delayed reepithelization and disordered collagen fibrillogenesis. *Matrix Biol* **28**, 65-73 (2009).
58 Wawersik, M. J., Mazzalupo, S., Nguyen, D. & Coulombe, P. A. Increased levels of keratin 16 alter epithelialization potential of mouse skin keratinocytes in vivo and ex vivo. *Molecular biology of the cell* **12**, 3439-3450 (2001).
59 Mazzalupo, S., Wawersik, M. J. & Coulombe, P. A. An ex vivo assay to assess the potential of skin keratinocytes for wound epithelialization. *J Invest Dermatol* **118**, 866-870 (2002).
60 Gat, U., DasGupta, R., Degenstein, L. & Fuchs, E. De Novo hair follicle morphogenesis and hair tumors in mice expressing a truncated beta-catenin in skin. *Cell* **95**, 605-614 (1998).
61 Liu, H. & Naismith, J. H. An efficient one-step site-directed deletion, insertion, single and multiple-site plasmid mutagenesis protocol. *BMC Biotechnol* **8**, 91, (2008).
62 Rendl, M., Lewis, L. & Fuchs, E. Molecular dissection of mesenchymal-epithelial interactions in the hair follicle. *PLoS Biol* **3**, 1910-1924 (2005).
63 Nelson, J. D., Denisenko, O. & Bomsztyk, K. Protocol for the fast chromatin immunoprecipitation (ChIP) method. *Nat Protoc* **1**, 179-185 (2006).

FIGURE LEGENDS

Figure 1. Tcf3 is induced at the wound edge and its overexpression promotes cell migration.

(A) Images of immunofluorescence analysis of wounded and unwounded skins of WT and *Tcf3* cKO skins show Tcf3 is induced at the wound edge of WT and not *Tcf3* cKO skins. Full thickness wounds were created on dorsal skins of 10-week old mice and isolated 5 days post wounding. Skins were analyzed by immunofluorescence with antibodies against Tcf3 (green) and keratin 5 (red). Wound-distant skin samples from the same mice were used as unwounded controls. Bar denotes 20μm.

(B) Images of keratinocytes 16hrs after the initiation of migration assay showing Tcf3-induced cells migrate more than control cells. Primary keratinocytes were isolated from tet-inducible Tcf3 (*K14rtTA;TRE-Tcf3)* or control (*K14-rtTA)* mice, grown to confluence, treated with doxycycline (Dox) or vehicle 24hrs prior to being subjected to the migration assay. Cells were treated with Mitomycin C for 2 hours to arrest proliferation, and a scratch was then made in the confluent monolayer using a pipet tip. The size of the scratch was measured at the beginning of the experiment and the area of cell migration was quantified after 16hrs using ImageJ software. Black bar denotes 200μM.

(C) Tcf3-induced cells show a 60% increase in migration compared with controls. Graph quantifying the area migrated by cells treated with Dox relative to the area migrated by cells treated with vehicle control. For each sample, over 30 non-overlapping fields were measured at each timepoint; and each experiment was repeated twice. Data are the mean ± s.e.m. **p<0.001.

(D) Tcf3 overexpression promotes cell migration in *ex vivo* skin explant culture. Graph quantifying the distance of outgrowth (μm) of epithelial cells from skin explants from control (*K14-rtTA)* or tet-inducible Tcf3 mice (*K14-rtTA;TRE-Tcf3)* that were treated with

vehicle or Dox at day 8 after plating. 4-mm dorsal skin punches were cultured for 8 days in the presence or absence of Dox and proliferation was blocked by Mitomycin C treatment on day 3. Explants from a minimum of 4 mice were analyzed for each condition.

(E) Representative images of epithelial outgrowth from explants that were immunostained with keratin 17 antibody and counterstained with hematoxylin after 8 days in culture. Bar denotes 1mm.

Figure 2. Tcf3 overexpression promotes wound healing.

(A) Images of skin wound sites taken 6 and 10 days post wounding. An area of $1cm^2$ full-thickness wounds were created on dorsal skins of tet-inducible Tcf3 (*K14-rtTA;TRE-mycTcf3*) or control (*K14-rtTA or TRE-mycTcf3*) mice that had been maintained on a doxycycline containing diet (n=5). 6 and 10 days after wounding, images of the wound sites were taken and the skins were embedded in OCT for analysis. The areas of the wounds are smaller in Tcf3-induced skins, indicating that Tcf3 expression accelerated wound repair.

(B) Graph quantifying the average area of the wounds 6 and 10 days post wounding show that wound closure was accelerated in Tcf3-induced skins. Areas of the wounds were measured with ImageJ software. Data are mean s.e.m. *$p<0.05$.

(C) H&E images of wounded skins from Tcf3-induced and control mice show faster re-epithelialization in the Tcf3-induced skin. Images of skins containing the wound sites were taken and merged using Panorama software. Open triangle indicates the edge of the reepithelialization sites. Black bar denotes 1mm.

(D) Graph quantifying the average width of the unrepaired wound sites based on H&E images. Data are mean s.e.m. *$p<0.05$.

Figure 3. Tcf3 induction in response to wounding is dependent on Stat3.

(A-B) Tcf3 and activated Stat3 (phospho-Y705) are induced at the wound edge in skin. Full-thickness wounds were created on dorsal skins of 10-week old mice and isolated 5 days post wounding. Skins containing the wound sites were analyzed by immunofluorescence with antibodies against phospho-Y705-Stat3 (red) and Tcf3 (Green). Unwounded skins from the same mice were used as controls.

(C-D) Ablation of Stat3 abolishes Tcf3 induction at the wound edge. Images of immunofluorescence analysis of the wound edge of skin from *Stat3*$^{fl/fl}$*;K14-Cre (Stat3* cKO*)* mice. Unwounded skins from the same mice were used as controls.

(E-F) Tcf3 mRNA is induced at the skin wound edge and its induction requires Stat3 expression. *In situ* hybridization analysis of Tcf3 expression at the wound edge of wild-type and *Stat3* ckO skin using antisense to *Tcf3* as probe (e) compared with Tcf3 sense as a control (f). Bar denotes 50μm.

(G) Constitutively activated Stat3 activates the *Tcf3* promoter. Keratinocytes were transfected with *Tcf3* promoter-Firefly luciferase and *Renilla* luciferase constructs, together with constructs expressing either Stat3, constitutively active Stat3 (Stat3C) or control vector. Luciferase activity was measured and Firefly luciferase activity was normalized over *Renilla* luciferase activity. Graph shows normalized luciferase activity relative to vector control. Experiments were repeated three times. Data are mean ± s.e.m. *$p<0.05$.

(H) Constitutively activated Stat3 activates the native *Tcf3* promoter but not a *Tcf3* promoter lacking conserved Stat3 binding sites. Keratinocytes were transfected with wild-type or mutated *Tcf3* promoter-Firefly luciferase and *Renilla* luciferase constructs, together with constructs expressing Stat3C or empty vector. Graph shows normalized luciferase activity relative to vector control. Experiments were repeated three times. Data are mean ± s.e.m. *$p<0.05$, **$p<0.01$.

(I) Endogenous Stat3 binds to the *Tcf3* promoter in epidermal cells. Chromatin immunoprecipitation (ChIP) was performed with anti-Stat3 or isotype control antibodies on crosslinked hair follicle cell chromatin lysate. Amount of chromatin precipitated by Stat3 or IgG was measured by qPCR using primers spanning regions containing Stat3 binding sites (sites 1-3) or regions without Stat3 conserved binding sites (neg cont). The graph shows the amount of fold enrichment of Stat3-immunoprecipitated DNA relative to IgG-immunoprecipitated DNA. Experiments were repeated three times. Data are mean ± s.e.m. *p<0.05.

Figure 4. Tcf3 induction rescues the defective migration in Stat3-deficient cells.

(A) Stat3-deficient cells have impaired cell migration which is reversed by the overexpression of Tcf3. Primary keratinocytes from *Stat3*$^{fl/fl}$ (cont) or *Stat3*$^{fl/fl}$*;K14-Cre (Stat3* cKO*)* mice were isolated and were transduced with GFP-tagged lentiviral vector expressing tet-inducible Tcf3 or with empty vector control. After the transduced cells were enriched by fluorescent cell sorting, they were grown to confluence and then subjected to a migration assay with or without Dox. Images of keratinocytes 48hrs after initiation of the migration assay. Black bar denotes 200μm.

(B) Graph quantifying the relative area the cells migrated normalized over vehicle control. For each sample, over 30 non-overlapping fields were measured at each timepoint; and each experiment was repeated three times. Data are the mean ± s.e.m. **p<0.001.

Figure 5. Tcf3 promotes cell migration non-cell autonomously and independently of its role as a cofactor to β-catenin.

(A) Real Time PCR analysis of level of expression of transduced tet-inducible Tcf3 and its mutant versions, Tcf3ΔN and Tcf3ΔG, in response to Dox. Keratinocytes were transduced with GFP-tagged, tet-inducible lentivectors carrying myc-tagged Tcf3 or its mutant versions. Transduced cells were isolated by fluorescent cell sorting and were treated with Dox or vehicle control for 24 hours prior to being harvested for mRNA analysis.

(B) The migration-promoting effect of Tcf3 relies on its interaction with Groucho/TLE corepressors and is independent of β-catenin. Images of transduced keratinocytes expressing tet-inducible Tcf3, Tcf3ΔN, Tcf3ΔG 16 hrs after the initiation of migration assay with or without Dox. Black bar denotes 200μm.

(C) Graph quantifying the area migrated by transduced cells treated with Dox relative to area migrated by cells treated with vehicle control. For each sample, over 30 non-overlapping fields were measured at each timepoint; and each experiment was repeated twice. Data are mean ± s.e.m. **p<0.001.

(D) Tcf3-induced cells secrete factors that promote cell migration. Keratinocytes from tet-inducible Tcf3 (*K14-rtTA;TRE-mycTcf3)* and control *(K14-rtTA)* mice were cultured in the presence or absence of Dox for 48 hours and their conditioned media were collected. Wild type keratinocytes were subjected to a migration assay in the presence of specified conditioned media. Images were taken 38hrs after the initiation of migration assay.

(E) Conditioned media from Tcf3-induced cells (*K14-rtTA;TRE-mycTcf3* +Dox) promotes migration of wild-type cells. Graph quantifying the migrated area of wild-type cells that were incubated with Dox treated conditioned media during the migration assay relative to the area migrated by cells treated with vehicle treated conditioned media. For each sample, over 30 non-overlapping fields were measured at each timepoint; and each experiment was repeated three times. Data are mean ± s.e.m. **p<0.001.

Figure 6. Lipocalin 2 is the key secreted mediator of Tcf3-induced cell migration and wound healing.

(A) Images of skin wound sites taken immediately after wounding and 10 days post wounding show that topical application of CM from Tcf3 overexpressing cells (Tcf3-CM) accelerates wound healing. After full-thickness wounds of $1cm^2$ were created on the dorsal skins of wild-type mice (n=5), CM from Tcf3-overexpressing cells or control cells was applied topically onto the wound sites daily for a week. Surface areas of the wounds were measured at the initial time point and 10 days post wounding.

(B) Graph quantifying the surface areas of the wounds as a percentage of the original wounds 10 days post wounding shows that CM from Tcf3-overexpressing cells (Tcf3-CM) accelerates wound closure. Data are mean ± s.e.m. *$p<0.05$.

(C) Tcf3 overexpression results in the induction of the secreted factor Lcn2. Real Time PCR analysis of Lcn2 expression in keratinocytes that were transduced to express tet-inducible Lef/Tcf members. Keratinocytes were transduced with GFP-tagged, tet-inducible lentivectors carrying myc-tagged Lef/Tcf members. Transduced cells were isolated by fluorescent cell sorting and were treated with Dox or vehicle control for 24 hours prior to being harvested for mRNA analysis.

(D) Inhibition of Lcn2 decreases the ability of Tcf3-CM to affect cell migration. Migration assays were performed on keratinocytes that were incubated with control CM or Tcf3-CM together with anti-Lcn2 antibody or IgG isotype control. Graph quantifying the relative area migrated by keratinocytes treated with Tcf3-CM incubated with IgG or anti-Lcn2 normalized over area migrated by cells treated with control CM. For each sample, over 30 non-overlapping fields were measured at each timepoint; and each experiment was repeated twice. Data are mean ± s.e.m. **$p<0.001$.

(E) Graph quantifying the surface areas of the wounds as a percentage of the original wounds 10 days post wounding shows that inhibition of Lcn2 decreases the ability of Tcf3-CM to promote wound healing. $1cm^2$ full-thickness wounds were created on dorsal skins of wild-type mice and were treated daily with topical application of conditioned media from control (empty vector) CM (cont-CM) (n=7) or Tcf3-CM untreated (n=7) or pre-incubated with antibodies against Lcn2 (n=8) or isotype control (n=6). Surface areas of the wounds were measured at the initial time point and 10 days post wounding. Data are mean ± s.e.m. *p<0.05.

(F) Lcn2 overexpression promotes cell migration. Migration assays were performed on keratinocytes that were incubated with Lcn2-CM or control (empty vector) CM (cont). Graph quantifying the relative migrated area of keratinocytes treated with the indicated CM. For each sample, over 30 non-overlapping fields were measured at each timepoint; and each experiment was repeated twice. Data are mean ± s.e.m. **p<0.001.

(G) Lcn2 accelerates wound closure. $1cm^2$ full-thickness wounds were created on dorsal skins of wild-type mice (n=4) and were treated daily with topical application of conditioned media (CM) from Lcn2 or control (empty vector) transduced keratinocytes. Images of the wound sites were taken at the beginning of the wounding experiment and 10 days post wounding, at which point skins were harvested for analysis.

(H) Graph quantifying the effect of topical application of Lcn2-CM on wound closure. Average surface areas of the wounds 10 days post wounding is quantified as a percentage of the initial wound areas. Areas of the wounds were measured with ImageJ software. Data are mean s.e.m. *p<0.05.

Figure 7. Lipocalin2 is required for efficient wound healing and can rescue defective wound healing in *Stat3* cKO mice.

(A) Images of skin wound sites taken immediately after wounding and 11 days post wounding show that topical application of antibodies against Lcn2 retarded wound healing. After full-thickness wounds of $1cm^2$ were created on the dorsal skins of *nude* mice (n=8), anti-Lcn2 or isotype control antibodies were applied topically onto the wound sites every other day. Surface areas of the wounds were measured at the initial time point and 11 days post wounding.

(B) Graph quantifying the surface areas of the wounds as a percentage of the original wounds 11 days post wounding shows that application of antibodies against Lcn2 retards wound closure. Data are mean ± s.e.m. *p<0.05.

(C) Inhibition of Lcn2 decreases the ability of Tcf3 to rescue defective migration in *Stat3* cKO keratinocytes. Migration assays were performed on *Stat3*$^{+/fl}$*:K14-cre* (cont) or *Stat3*$^{fl/fl}$*:K14-cre* (*Stat3* cKO) keratinocytes that were transduced with control or tet-inducible Tcf3 treated with Dox together with anti-Lcn2 antibody or IgG isotype control. Graph quantifying the relative area migrated by keratinocytes normalized over area migrated by cells transduced with control vector without Dox. For each sample, over 30 non-overlapping fields were measured at each timepoint; and each experiment was repeated twice. Data are mean ± s.e.m. **p<0.001.

(D) Images of skin wound sites taken 10 days post wounding show that topical application of recombinant Lcn2 rescues defective wound healing in *Stat3* cKO mice. After full-thickness wounds of $1cm^2$ were created on the dorsal skins of wild-type (n=13) and *Stat3* cKO (n=11) mice, 200µl of recombinant Lcn2 (2µg/ml) or vehicle were applied topically onto the wound sites every other day. Surface areas of the wounds were measured at the initial time point and 10 days post wounding.

(E) Graph quantifying the surface areas of the wounds as a percentage of the original wounds 10 days post wounding shows that Lcn2 rescues wound closure defect in *Stat3* cKO mice. Data are mean ± s.e.m. *p<0.05 and **p<0.001.

Miao_Fig1

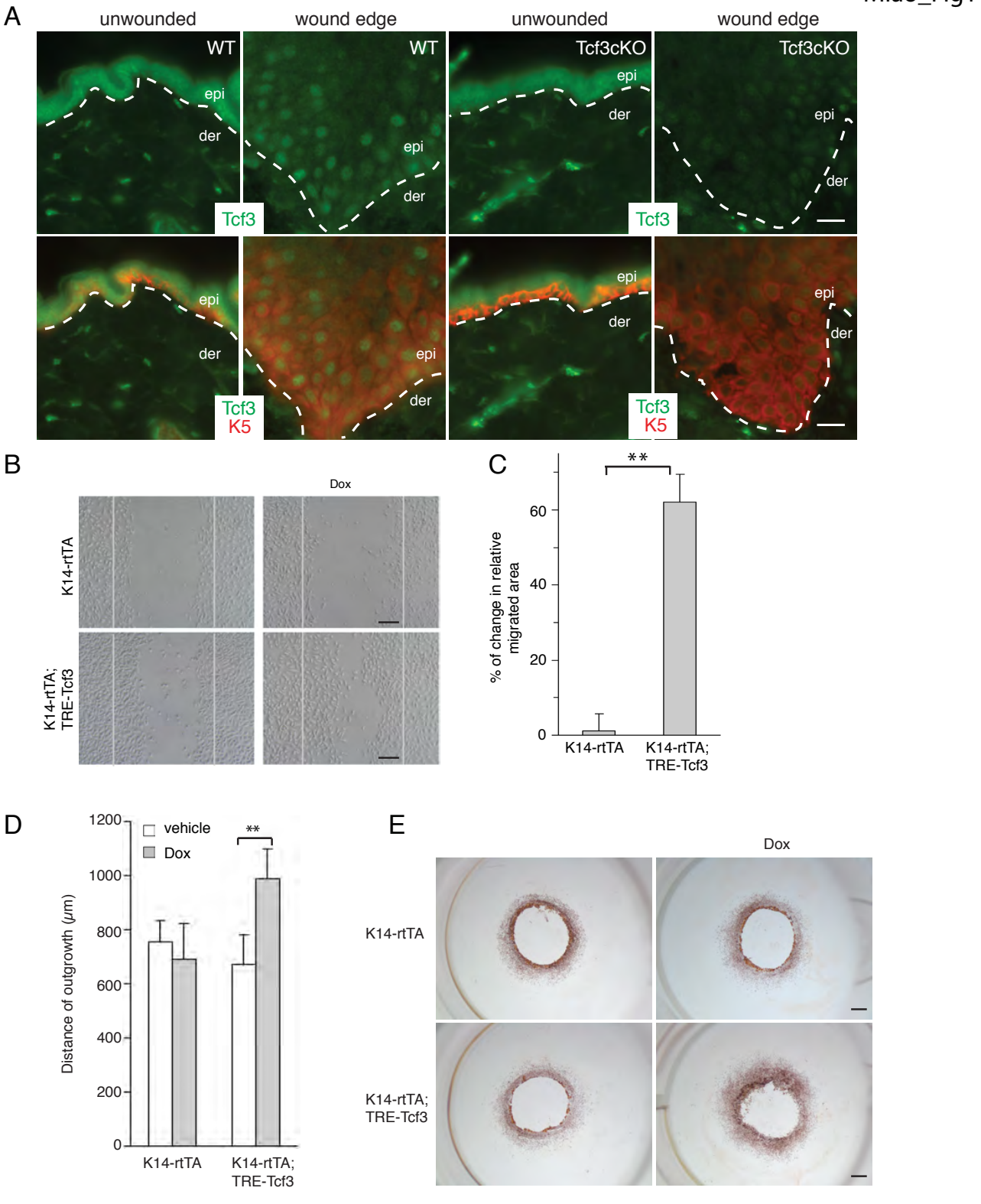
A
unwounded
wound edge
unwounded
wound edge
WT
WT
Tcf3cKO
Tcf3cKO
epi
der
Tcf3
Tcf3
K5
B
Dox
K14-rtTA
K14-rtTA;
TRE-Tcf3
C
**
% of change in relative migrated area
60
40
20
0
K14-rtTA
K14-rtTA;
TRE-Tcf3
D
vehicle
Dox
**
Distance of outgrowth (μm)
1200
1000
800
600
400
200
0
K14-rtTA
K14-rtTA;
TRE-Tcf3
E
Dox
K14-rtTA
K14-rtTA;
TRE-Tcf3

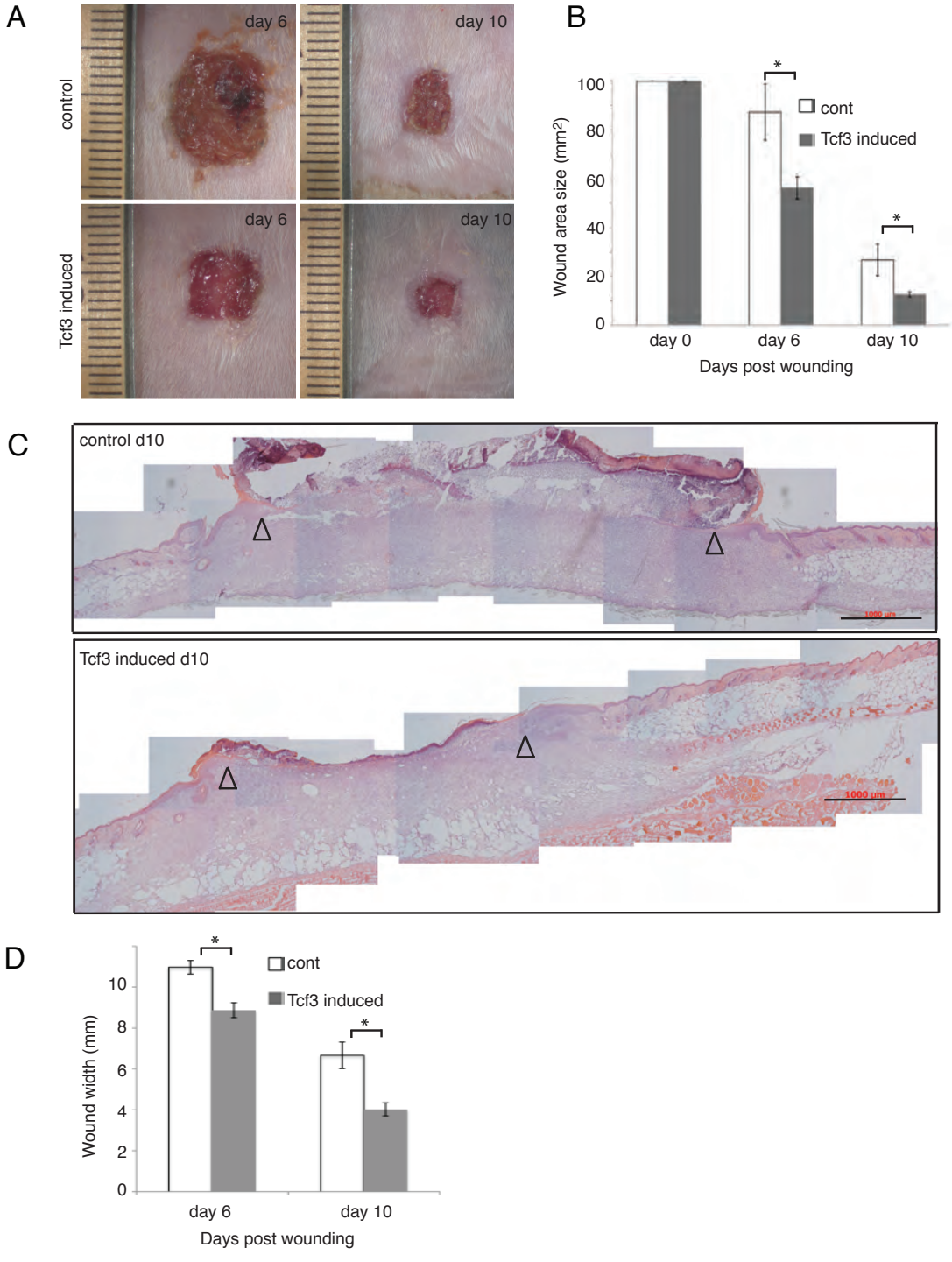
A
day 6
day 10
control
day 6
day 10
Tcf3 induced
B
Wound area size (mm2)
100
80
60
40
20
0
cont
Tcf3 induced
*
*
day 0
day 6
day 10
Days post wounding
C
control d10
Tcf3 induced d10
1000 µm
1000 µm
D
Wound width (mm)
10
8
6
4
2
0
cont
Tcf3 induced
*
*
day 6
day 10
Days post wounding

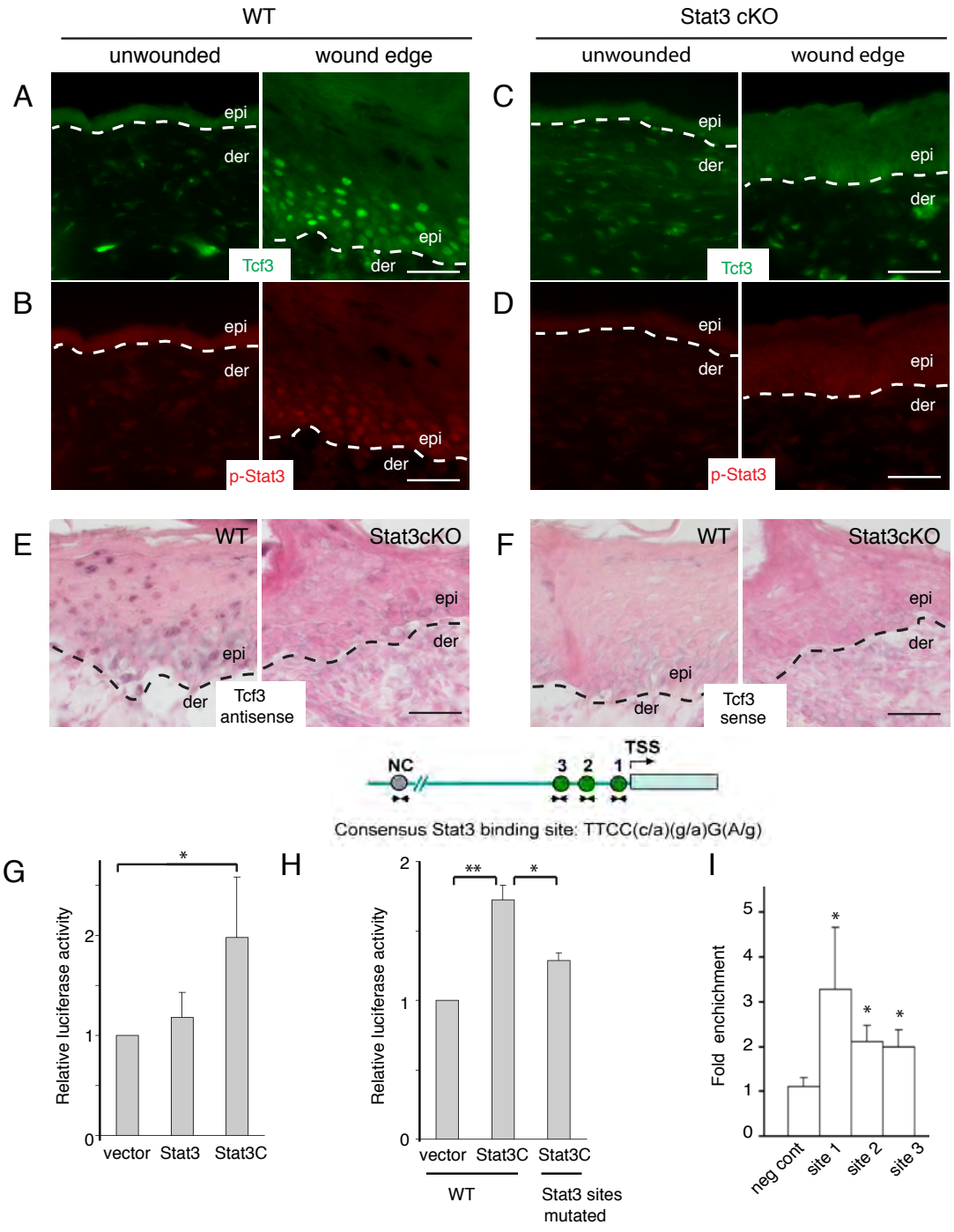
WT
Stat3 cKO
unwounded
wound edge
unwounded
wound edge
A
B
C
D
epi
der
Tcf3
p-Stat3
E
F
WT
Stat3cKO
Tcf3
antisense
Tcf3
sense
NC
TSS
3
2
1
Consensus Stat3 binding site: TTCC(c/a)(g/a)G(A/g)
G
Relative luciferase activity
vector
Stat3
Stat3C
H
Relative luciferase activity
vector
Stat3C
Stat3C
WT
Stat3 sites
mutated
I
Fold enrichment
neg cont
site 1
site 2
site 3

Miao_Fig4

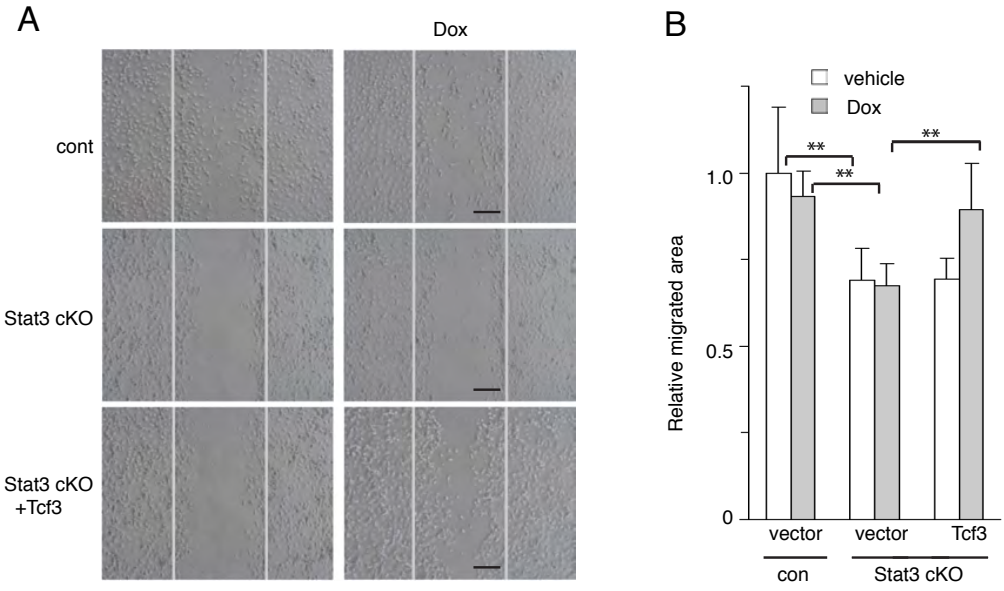
A
Dox
cont
Stat3 cKO
Stat3 cKO
+Tcf3
B
vehicle
Dox
**
**
**
1.0
0.5
0
Relative migrated area
vector
vector
Tcf3
con
Stat3 cKO

Miao_Fig5

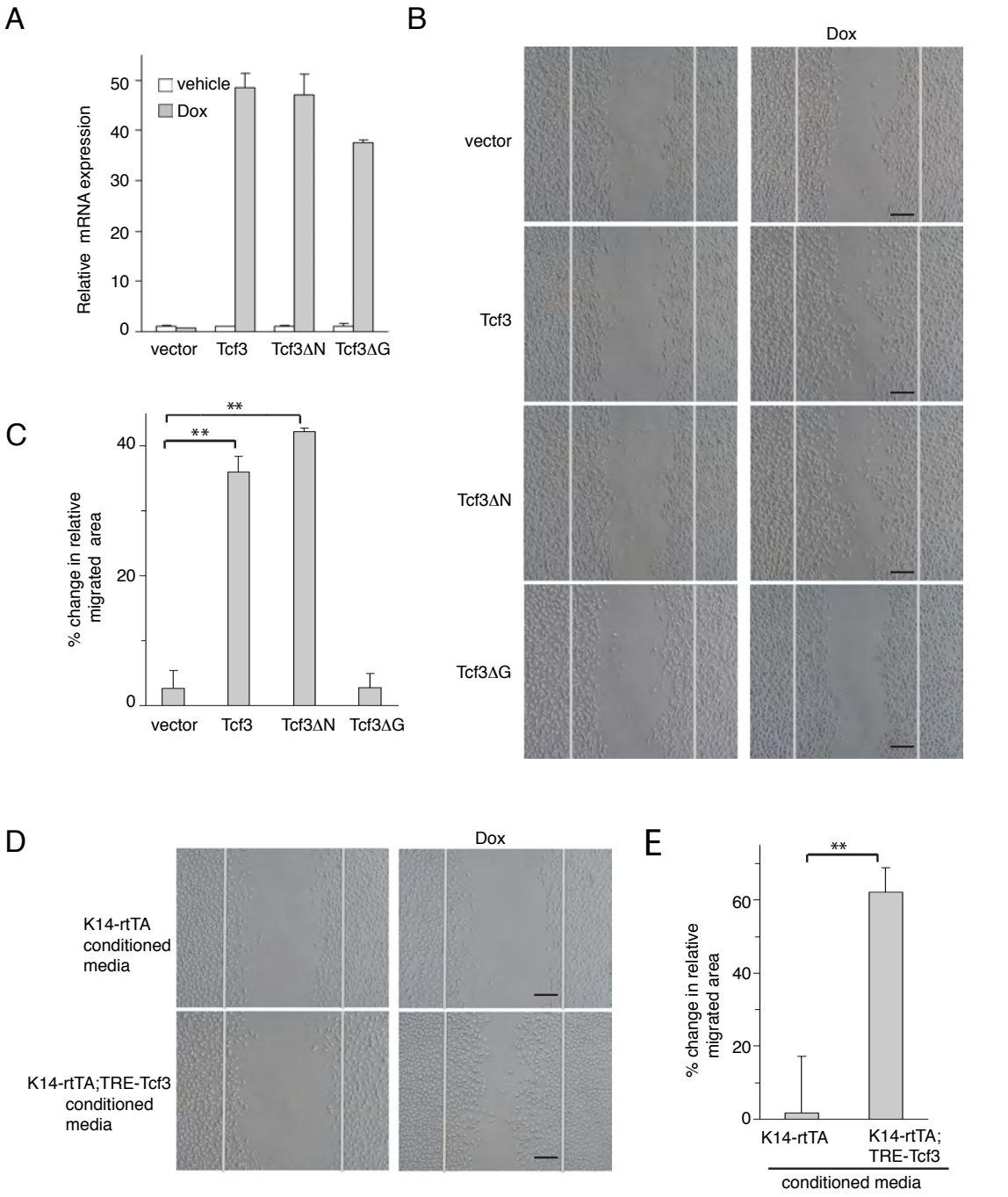
A
vehicle
Dox
Relative mRNA expression
50
40
30
20
10
0
vector
Tcf3
Tcf3ΔN
Tcf3ΔG
B
Dox
vector
Tcf3
Tcf3ΔN
Tcf3ΔG
C
**
**
% change in relative migrated area
40
20
0
vector
Tcf3
Tcf3ΔN
Tcf3ΔG
D
Dox
K14-rtTA conditioned media
K14-rtTA;TRE-Tcf3 conditioned media
E
**
% change in relative migrated area
60
40
20
0
K14-rtTA
K14-rtTA; TRE-Tcf3
conditioned media

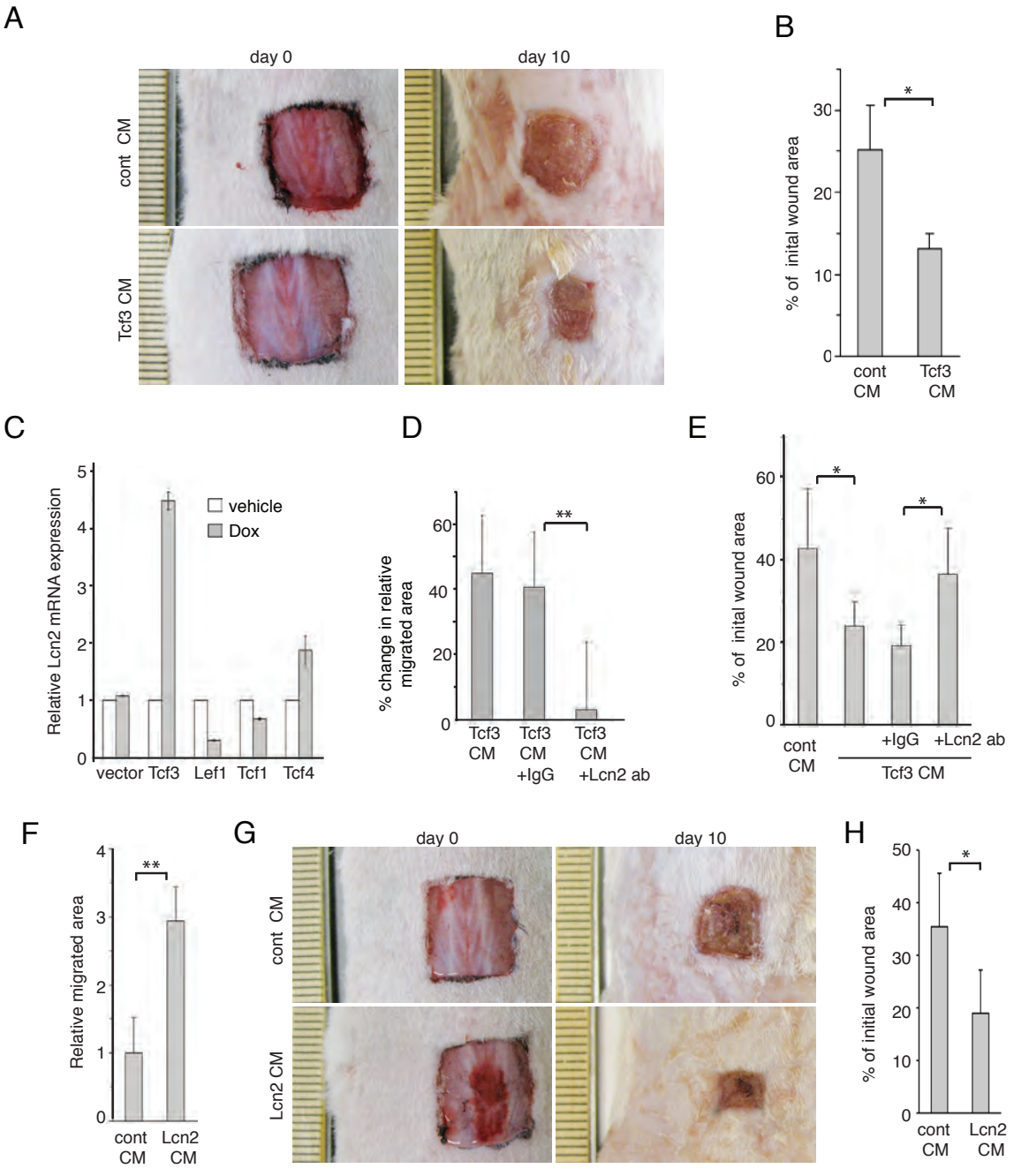
A
day 0
day 10
cont CM
Tcf3 CM
B
% of inital wound area
cont CM
Tcf3 CM
C
Relative Lcn2 mRNA expression
vehicle
Dox
vector
Tcf3
Lef1
Tcf1
Tcf4
D
% change in relative migrated area
Tcf3 CM
Tcf3 CM +IgG
Tcf3 CM +Lcn2 ab
E
% of inital wound area
cont CM
+IgG
+Lcn2 ab
Tcf3 CM
F
Relative migrated area
cont CM
Lcn2 CM
G
day 0
day 10
cont CM
Lcn2 CM
H
% of initial wound area
cont CM
Lcn2 CM

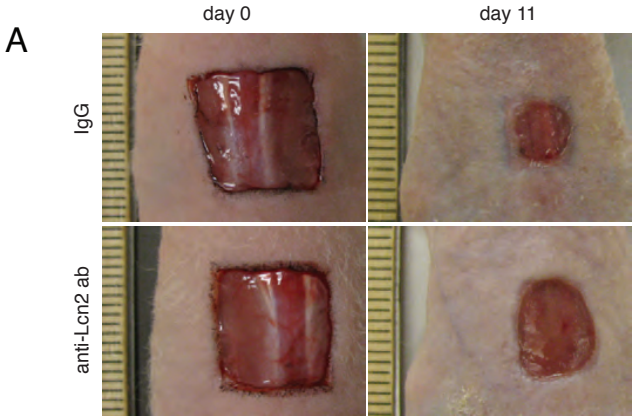
A
day 0
day 11
IgG
anti-Lcn2 ab

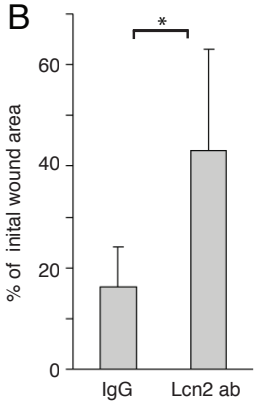
B
*
60
40
20
0
% of inital wound area
IgG
Lcn2 ab

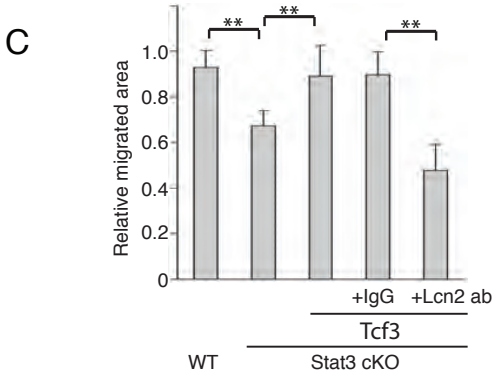
C
**
**
**
1.0
0.8
0.6
0.4
0.2
0
Relative migrated area
+IgG
+Lcn2 ab
Tcf3
WT
Stat3 cKO

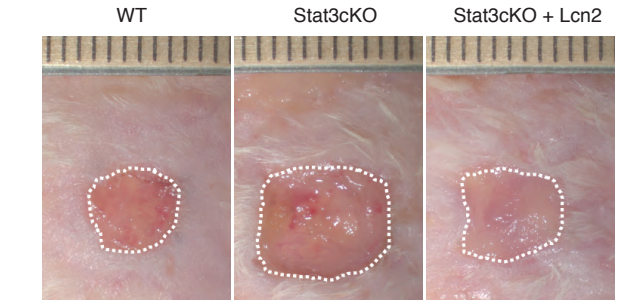
D
WT
Stat3cKO
Stat3cKO + Lcn2

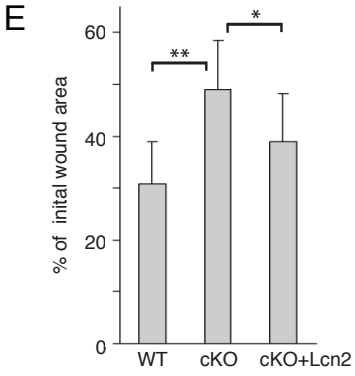
E
**
*
60
40
20
0
% of inital wound area
WT
cKO
cKO+Lcn2